

Updated Constraints and Forecasts on Primordial Tensor Modes

Giovanni Cabass,¹ Luca Pagano,¹ Laura Salvati,¹ Martina Gerbino,^{2,3,1} Elena Giusarma,^{4,1} and Alessandro Melchiorri¹

¹*Physics Department and INFN, Università di Roma “La Sapienza”, P.le Aldo Moro 2, 00185, Rome, Italy*

²*The Oskar Klein Centre for Cosmoparticle Physics, Department of Physics, Stockholm University, AlbaNova, SE-106 91 Stockholm, Sweden*

³*Nordita (Nordic Institute for Theoretical Physics), Roslagstullsbacken 23, SE-106 91 Stockholm, Sweden*

⁴*McWilliams Center for Cosmology, Department of Physics, Carnegie Mellon University, Pittsburgh, PA 15213, USA.*

We present new, tight, constraints on the cosmological background of gravitational waves (GWs) using the latest measurements of CMB temperature and polarization anisotropies provided by the *Planck*, BICEP2 and *Keck Array* experiments. These constraints are further improved when the GW contribution $N_{\text{eff}}^{\text{GW}}$ to the effective number of relativistic degrees of freedom N_{eff} is also considered. Parametrizing the tensor spectrum as a power law with tensor-to-scalar ratio r , tilt n_t and pivot 0.01 Mpc^{-1} , and assuming a minimum value of $r = 0.001$, we find $r < 0.089$, $n_t = 1.7_{-2.0}^{+2.1}$ (95% CL, no $N_{\text{eff}}^{\text{GW}}$) and $r < 0.082$, $n_t = -0.05_{-0.87}^{+0.58}$ (95% CL, with $N_{\text{eff}}^{\text{GW}}$). When the recently released 95 GHz data from *Keck Array* are added to the analysis, the constraints on r are improved to $r < 0.067$ (95% CL, no $N_{\text{eff}}^{\text{GW}}$), $r < 0.061$ (95% CL, with $N_{\text{eff}}^{\text{GW}}$). We discuss the limits coming from direct detection experiments such as LIGO-Virgo, pulsar timing (European Pulsar Timing Array) and CMB spectral distortions (FIRAS). Finally, we show future constraints achievable from a CORe-like mission: if the tensor-to-scalar ratio is of order 10^{-2} and the inflationary consistency relation $n_t = -r/8$ holds, CORe will be able to constrain n_t with an error of 0.16 at 95% CL. In the case that lensing B -modes can be subtracted to 10% of their power, a feasible goal for CORe, these limits will be improved to 0.11 at 95% CL.

PACS numbers: 98.80.Bp, 98.80.Cq, 98.80.Es, 98.80.Jk, 98.80.Ft, 98.70.Vc

I. INTRODUCTION

After the impressive confirmation of the standard Λ CDM model of structure formation by many ground, balloon and space experiments [1–4], the search for primordial gravitational waves (GWs) is one of the main goals of modern cosmology. Long-wavelength gravitational waves are predicted by the current go-to theory for the solution to the horizon and flatness problems of the Hot Big Bang picture (and the generation of primordial density perturbations), *i.e.* cosmic inflation [5–7]. The scale at which inflation occurs is related to the amount of primordial tensor power, while the simplest models (with a single degree of freedom parametrizing the evolution of the inflationary energy density) predict the tensor spectrum to be slightly red-tilted (see [8] for a comprehensive review). Constraining the tensor amplitude and tilt, then, will be an important step in the discrimination between different models of the early universe (see e.g. [9] for a recent review).

In this paper we update the constraints on the parameters describing the tensor spectrum $P_t(k)$ in light of the *Planck* 2015 data [10], the measurement of the BB spectrum from the BICEP2/*Keck-Planck* (hereafter BKP) combined analysis [11], and the recently released 95 GHz data from *Keck Array* [12]. We consider a power law parametrization of $\Delta_t^2(k) \equiv k^3 P_t(k)/2\pi^2$ in terms of

the tensor amplitude A_t and the tilt n_t , *i.e.*

$$\Delta_t^2(k) = A_t \left(\frac{k}{k_*} \right)^{n_t}, \quad (1)$$

where A_t is the amplitude of the tensor power spectrum at the pivot scale k_* . The scalar spectrum $\Delta_s^2(k)$ will be analogously parametrized in terms of its amplitude and the spectral index n_s , *i.e.*

$$\Delta_s^2(k) = A_s \left(\frac{k}{k_*} \right)^{n_s-1}, \quad (2)$$

and we will consider the tensor-to-scalar ratio $r \equiv A_t/A_s$ in place of A_t in the following analysis.

It is well known that the sensitivity of Cosmic Microwave Background (CMB) experiments to $P_t(k)$ comes from the contribution of primordial tensor modes to the angular power spectra of the CMB temperature and polarization anisotropies, *i.e.*

$$C_\ell^{XY,t} = \int_0^{+\infty} \frac{dk}{k} \Delta_{\ell,X}^t(k) \Delta_{\ell,Y}^t(k) P_t(k), \quad (3)$$

where $\Delta_{\ell,X}^t(k)$ are the transfer functions ($X = T, E, B$) for tensor modes, dependent on late-time physics. The accurate measurement of T , E and B anisotropies from the *Planck* experiment at large scales, together with the limit on B -mode polarization from the BKP joint analysis, has allowed to obtain $r_{0.002} < 0.08$ at 95% CL (*Planck* TT + lowP + BKP dataset: see [13]).

Measurements of CMB anisotropies alone, however, are limited to scales k from $\approx 10^{-3} \text{Mpc}^{-1}$ to $\approx 10^{-1} \text{Mpc}^{-1}$: a much larger range of scales becomes available when one considers the following experiments, also sensitive to primordial GWs [14–16] (see figure A2 of [17] for details about sensitivities) :

- direct detection experiments, such as LIGO [18, 19], and Virgo [20, 21]. With these ground-based interferometers one can probe the primordial gravitational wave spectrum in a range of frequencies Δf (with $2\pi f = ck$) from $\sim 1 \text{Hz}$ to $\sim 10^4 \text{Hz}$, while the planned space-based eLISA [22, 23], DECIGO [24, 25] and the proposed Big-Bang Observer (BBO) [26] focus on frequencies from $\sim 10^{-4} \text{Hz}$ to $\sim 1 \text{Hz}$;
- high-stability pulsar timing experiments, like the European Pulsar Timing Array (EPTA) [27], which are sensitive to GWs in frequencies between $\sim 10^{-9} \text{Hz}$ and $\sim 10^{-7} \text{Hz}$;
- measurements of the CMB energy spectrum [28]: two recent papers [29, 30] showed how the integrated tensor power from $k \approx 10^3 \text{Mpc}^{-1}$ ($f \approx 10^{-12} \text{Hz}$) to $k \approx 10^6 \text{Mpc}^{-1}$ ($f \approx 10^{-9} \text{Hz}$) gives a contribution to the spectral distortions of the CMB spectrum, subleading with respect to distortions caused by Silk damping of acoustic waves in the baryon-photon fluid [31–33] (which, conversely, allow to probe the integrated spectrum of scalar perturbations [34, 35]).

For a visual impression of the various scales probed by these different observables see the illustrative plot Fig. 1.

In addition to this, primordial gravitational waves have also an effect on the expansion of the universe: being relativistic degrees of freedom, they will add to the effective number of relativistic species N_{eff} [36, 37], increase the radiation energy density, and therefore decrease the redshift of matter-radiation equality, as one can see from the relation

$$1 + z_{\text{eq}} = \frac{\Omega_{\text{m}}}{\Omega_{\text{r}}} = \frac{\Omega_{\text{m}}}{\Omega_{\gamma}(1 + 0.2271N_{\text{eff}})}. \quad (4)$$

This alters the CMB power spectrum in a way similar to that of additional sterile, massless neutrinos (see [38, 39] and references therein for an analysis of these effects).

The contribution to the radiation content of the universe will also affect primordial nucleosynthesis (BBN). A larger amount of gravitational waves will result in a more rapid expansion of the universe: this, in turn, means that neutrons will have less time to decay before the freeze-out of weak interactions, leading to a larger neutron-to-proton ratio and an overproduction of helium. One can then consider the astrophysical constraints on the abundances of light elements like helium [40, 41] and Deuterium [42], and the effect that altering the value of the primordial helium abundance Y_{P} has on the CMB angular power spectrum [43, 44].

Several authors have used these observables to provide constraints on both the primordial and not primordial

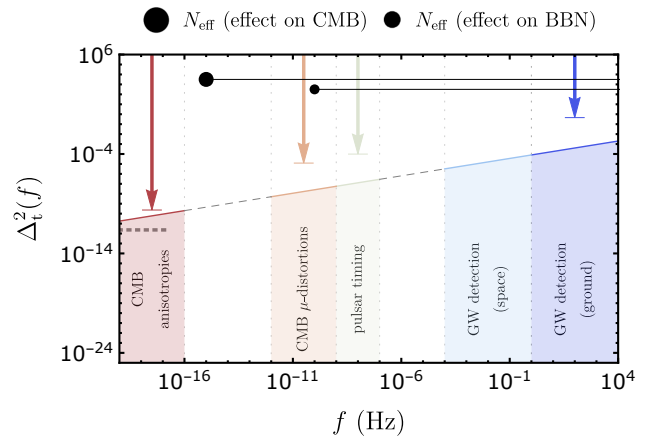


FIG. 1. Cartoon plot of a power-law (blue) primordial tensor spectrum ($\Delta_{\text{t}}^2 = 10^{-10}$, $n_{\text{t}} = 0.35$) over a range of frequencies f going from 10^{-17}Hz (smallest frequency that can be probed with CMB anisotropies) to 10^4Hz (largest frequency available to ground-based experiments). The vertical arrows represent the current upper bounds on the tensor amplitude at different scales. We show with a gray dotted line the prior on r used in our analysis ($r > 0.001$). The filled regions show which is the relevant Δf for the various observables discussed in the text. We refer to Sec. II A for a more accurate discussion regarding primordial abundances and the effect on CMB anisotropies. We stress that this plot has only illustrative purposes.

(*e.g.* the possible contribution coming from networks of cosmic strings [45, 46]) gravitational wave spectrum [47–62]. We note that in most of these works the tensor-to-scalar ratio r is fixed at a reference value: if this value is high enough (*e.g.* of order 10^{-1}), this will result in more stringent constraints on the tilt (see, *e.g.*, [52]). In our case, instead, we consider r as a free parameter, varying along with the tilt.

Before going on, we highlight which are the main novelties of this work:

- we include the recent B -mode polarization data coming from the BICEP2 and *Keck Array* experiments [12] that improve significantly the constraints on the tensor mode amplitude r ;
- we examine which limits can be obtained from CMB μ -distortions. While the current sensitivity (the state of the art being the FIRAS instrument on the COBE satellite) is too low for this observable to be competitive with the other ones discussed in the text, we note that this is a “pure CMB” constraint on the tilt, in the sense that no other observable besides the Cosmic Microwave Background is used to obtain it. Besides, one has to keep in mind that future experiments like PIXIE [63] and LiteBIRD [64] are planned to have order 10^3 times the sensitivity of FIRAS: therefore the limits from spectral distortions that we obtain in this paper will certainly be improved;
- we explicitly include in our analysis the above mentioned effect of gravitational waves on Y_{P} and the

bound on N_{eff} from the observations of light element abundances;

- we perform a forecast on the parameters r and n_t combining future CMB experiments like CORe [65] and GW direct detection experiments as AdvLIGO [66]. We consider a fiducial cosmology where the tensor-to-scalar ratio is of order 10^{-2} , with tilt fixed by the single-field slow-roll consistency relation $n_t = -r/8$. Such values of r will be probed by ground-based experiments like AdvACT [67], a new receiver for the Atacama Cosmology Telescope based on projected improvements of the existing ACTPol camera [68]. The reason for this analysis is the following: if primordial tensor modes are detected, and there is no more the freedom of changing the overall scale of the spectrum, constraining its scale dependence will be one of the main goals of future B -mode cosmology [69];
- we include delensing in our forecasts: recently it has been shown that lensing B -modes can be subtracted to 10% of their original power if noise is brought down to $\approx 1 \mu\text{K} \cdot \text{arcmin}$ [70]. In this case, a larger range of multipoles becomes available to probe the scale dependence of the B -mode spectrum from tensors, leading to stronger constraints on n_t : we refer to Sec. III C for details.

The paper is organized as follows: the next section contains a more detailed description on the observables introduced above. In Sec. III we present our data analysis and forecasting methods, in Sec. IV we discuss our results and we draw our conclusions in Sec. V.

II. GW SPECTRUM AND OBSERVATIONS

The spectrum of primordial gravitational waves, at the present time and at a given frequency $f = k/2\pi$ (we take $a(\eta_0) = 1$), is given by [47, 52, 71]

$$\Omega_{\text{GW}}(f) \equiv \frac{1}{\rho_c} \frac{d\rho_{\text{GW}}}{d \log f} = \frac{\Delta_t^2(f)}{24z_{\text{eq}}}, \quad (5)$$

where $\rho_c = 3H^2/8\pi G$ is the critical density. This expression is found by solving the evolution equation for the gravitational wave amplitude in an expanding universe: for a detailed treatment of transfer functions for tensor perturbations, see [72, 73].

Plugging in numerical values (*i.e.* $f/\text{Hz} = 1.6 \times 10^{-15} k/\text{Mpc}^{-1}$), we obtain

$$\begin{aligned} \Delta_t^2(f) &= r A_s \left(\frac{f}{f_\star} \right)^{n_t} \\ &= r A_s \left(\frac{f/\text{Hz}}{1.6 \times 10^{-17}} \right)^{n_t}. \end{aligned} \quad (6)$$

for a pivot scale $k_\star = 0.01 \text{ Mpc}^{-1}$.

Starting from this formula, we can discuss the impact that GWs have on the various observables that will be used in our analysis, starting from the effects on nucleosynthesis and the abundances of primordial elements.

A. Nucleosynthesis and primordial abundances

The gravitational wave contribution to the number of relativistic degrees of freedom $g_*(T)$ at temperature T is given by:

$$g_*^{(\text{GW})}(T) = 2 \left(\frac{T_{\text{GW}}}{T_\gamma} \right)^4 = 2 \frac{\rho_{\text{GW}}}{\rho_\gamma}, \quad (7)$$

where the factor of 2 comes from the two helicities of tensor perturbations. At temperatures $T \gtrsim 1 \text{ MeV}$, when the relativistic degrees of freedom are e^\pm, γ, ν and GWs, expressing $g_*(T)$ in terms in the effective number of neutrino species $N_{\text{eff}}^{\text{GW}} = 3.046 + N_{\text{eff}}^{\text{GW}}$ gives

$$N_{\text{eff}}^{\text{GW}} = \frac{8}{7} \frac{\rho_{\text{GW}}}{\rho_\gamma}. \quad (8)$$

In order to relate this to Eq. (5), which involves the spectrum of primordial gravitational waves at the present time, one notes that from $T \gtrsim 1 \text{ MeV}$ to the present time ρ_{GW} scales as a^{-4} , while the photon energy density evolves as $\rho_\gamma \sim 1/(a^4 g_{*,s}^{4/3})$ (*i.e.* by keeping entropy constant). The result is:

$$N_{\text{eff}}^{\text{GW}} = \frac{8}{7} \left(\frac{g_{*,s}(T \gtrsim 1 \text{ MeV})}{g_{*,s}(T_0)} \right)^{\frac{4}{3}} \frac{\rho_{\text{GW}}}{\rho_\gamma} \Big|_{\eta=\eta_0}, \quad (9)$$

where T_0 is the temperature of the CMB at the present time $\eta = \eta_0$. Multiplying both ρ_{GW} and ρ_γ by $1/\rho_c$, and using the definition of $\Omega_{\text{GW}}(f)$ given in Eq. (5), one obtains:

$$N_{\text{eff}}^{\text{GW}} = \frac{8}{7} \left(\frac{g_{*,s}(T \gtrsim 1 \text{ MeV})}{g_{*,s}(T_0)} \right)^{\frac{4}{3}} \frac{\rho_c}{\rho_\gamma} \int_0^{+\infty} d \log f \Omega_{\text{GW}}(f). \quad (10)$$

Inserting numerical values one can find [15, 50, 61]:

$$N_{\text{eff}}^{\text{GW}} \approx \frac{h_0^2}{5.6 \times 10^{-6}} \int_0^{+\infty} d \log f \Omega_{\text{GW}}(f). \quad (11)$$

If, instead of considering temperatures $T \gtrsim 1 \text{ MeV}$, one starts from times around decoupling (relevant for how N_{eff} affects the CMB spectra), one can find that the expression of $N_{\text{eff}}^{\text{GW}}$ in terms of ρ_{GW} is the same as that of Eqs. (10) and (11).

In the above equations the gravitational wave spectrum is integrated over all frequencies, from $f = 0$ to $f = +\infty$. In reality there are both IR and UV cutoffs to this integral:

- the IR cutoff comes from the fact that the only gravitational waves that contribute to the radiation energy

density at a given time $\bar{\eta}$ are those inside the horizon at $\eta = \bar{\eta}$. In fact these are the ones that have begun to oscillate, and then propagate as massless modes [74, 75]. This means that we have to consider two different $N_{\text{eff}}^{\text{GW}}$:

1. the first one is $N_{\text{eff,BBN}}^{\text{GW}}$, the contribution of GWs to N_{eff} that will enter in the computation of the abundances of primordial elements. Its IR cutoff will be the frequency corresponding to the horizon size at the time of nucleosynthesis, *i.e.* $\approx 10^{-12}$ Hz. Actually we take the cutoff to be of order 10^{-10} Hz, since, realistically, the gravitational waves will need to oscillate for a while after entering the horizon before contributing to ρ_{rad} , see for details figure 2 of [74] and [50, 76];
2. the second one is $N_{\text{eff,CMB}}^{\text{GW}}$, that will affect the CMB power spectra through its effect on the redshift of matter-radiation equality and the comoving sound horizon. Its IR cutoff will be the horizon size at decoupling. This would be given by $\approx 10^{-17}$ Hz, but we take it to be of order 10^{-15} Hz for the same reason as before [50].

The two contributions to N_{eff} will differ a lot from each other only in the case of very red tensor spectra (when the resulting $N_{\text{eff}}^{\text{GW}}$ is too small to have an effect anyway): for blue spectra the dependence of ρ_{GW} on the IR cutoff is very weak;

- the UV cutoff is more arbitrary: if gravitational waves are produced by inflation, we expect a cutoff corresponding to the horizon size k_{end} ($\approx 10^{23} \text{ Mpc}^{-1}$ for GUT-scale inflation and instant reheating - see Sec. VIA for a derivation) at the end of inflation, since GWs of smaller wavelength will not be produced. Other authors make different choices for UV cutoff, without referring to the inflationary theory [58]: for example one can suppose to have a production of gravitational waves up to the horizon size before the ≈ 60 e-folds of hot Big Bang expansion. In [52], instead, the authors choose the UV cutoff to be given by the Planck frequency, *i.e.* $f_{\text{P}} \approx 1/t_{\text{P}} = 10^{43} \text{ Hz}$ (with $k_{\text{P}} \approx 10^{57} \text{ Mpc}^{-1}$). Among these options, we choose $k_{\text{UV}} = k_{\text{end}} \approx 10^{23} \text{ Mpc}^{-1}$: this allows to be more conservative with the constraints on the tensor tilt, since for a given n_t , a larger UV cutoff will result in a larger $N_{\text{eff}}^{\text{GW}}$. There are still some caveats to this argument, however, since the scale of the end of inflation is not determined unless the details of the transition to radiation dominance are specified: we refer to Sec. V for a more complete discussion.

We conclude this section by noting that the integral in Eq. (11) can be carried out analytically, giving (for $h_0^2 \approx 0.5$, a pivot of 0.01 Mpc^{-1} , and taking $f_{\text{UV}} = ck_{\text{end}}/2\pi =$

$3.1 \times 10^8 \text{ Hz}$)

$$\begin{aligned} N_{\text{eff,BBN}}^{\text{GW}} &\approx 3 \times 10^{-6} \times \frac{rA_s}{n_t} \left[\left(\frac{f}{f_*} \right)^{n_t} \right]_{10^{-10} \text{ Hz}}^{3 \times 10^8 \text{ Hz}}, \\ &\approx 3 \times 10^{-6} \times \frac{rA_s}{n_t} \times (10^{25n_t} - 10^{7n_t}), \end{aligned} \quad (12a)$$

$$\begin{aligned} N_{\text{eff,CMB}}^{\text{GW}} &\approx 3 \times 10^{-6} \times \frac{rA_s}{n_t} \left[\left(\frac{f}{f_*} \right)^{n_t} \right]_{10^{-15} \text{ Hz}}^{3 \times 10^8 \text{ Hz}}, \\ &\approx 3 \times 10^{-6} \times \frac{rA_s}{n_t} \times (10^{25n_t} - 63^{n_t}). \end{aligned} \quad (12b)$$

B. CMB distortions

Once the tight-coupling approximation breaks down, the anisotropic stresses in the photon-baryon plasma become manifest, generating the dissipation of acoustic waves by Silk damping: at redshifts above $z \approx 2 \times 10^6 \equiv z_{\mu,i}$, this energy released in the plasma is thermalized successfully by processes like elastic and double Compton scattering ($e^- + \gamma \rightarrow e^- + 2\gamma$), resulting again in a black-body spectrum with a higher temperature [77]. At redshift between $z_{\mu,i}$ and $z \approx 5 \times 10^4 \equiv z_{\mu,f}$, elastic Compton scattering allows to still achieve equilibrium, but photon number changing processes are frozen out due to the cosmic expansion and cannot re-establish a black-body spectrum. The result is a perturbed Planck spectrum that can be approximated by a Bose-Einstein distribution $1/(e^{x+\mu(x)} - 1)$ ($x \equiv h\nu/k_{\text{B}}T$), where $\mu(x)$ can be identified as a chemical potential, independent on frequency away from the Rayleigh-Jeans tail [78].

The photon quadrupole anisotropy plays a crucial role in this dissipation process, giving rise to shear viscosity in the photon fluid [79, 80]. It is not, however, the only source of energy injection: the local quadrupole anisotropy is also sourced by tensor perturbations, without the need of photon diffusion [81]. Thomson scattering then mixes photons causing nearly scale independent dissipation [29, 30].

Using the Bose-Einstein distribution $1/(e^{x+\mu(x)} - 1)$ plus the fact that, for $z_{\mu,f} \lesssim z \lesssim z_{\mu,i}$, the total number of photons is constant, one can show that for an amount of energy (density) δE released into the plasma the resulting μ -distortion is

$$\mu = 1.4 \int_{z_{\mu,i}}^{z_{\mu,f}} dz \frac{d(Q/\rho_\gamma)}{dz}, \quad (13)$$

where $d(Q/\rho_\gamma)/dz$ is the energy injection as a function of redshift: $d(Q/\rho_\gamma)/dz$ will be also be a function of position, *i.e.* there will be inhomogeneities in the chemical potential μ . If we focus on the μ -monopole $\langle \mu \rangle$, instead, one can show that:

- for scalars, $\langle d(Q/\rho_\gamma)/dz \rangle$ is

$$\left\langle \frac{d(Q/\rho_\gamma)}{dz} \right\rangle_s = \frac{9}{0.4R_\nu + 1.5} \frac{d(k_d^{-2})}{dz} \times \int_0^{+\infty} \frac{d^3 k}{4\pi} \frac{\Delta_s^2(k)}{k} e^{-2k^2/k_d^2}, \quad (14)$$

where $R_\nu = \rho_\nu/(\rho_\nu + \rho_\gamma)$ is approximately 0.41. The damping wavenumber k_d is related to the mean squared diffusion distance r_d simply by $k_d = \pi/r_d$, while r_d is given by

$$r_d^2 = \pi^2 \int_0^a \frac{da'}{a'^3 \sigma_T n_e H} \left[\frac{R^2 + \frac{16}{15}(1+R)}{6(1+R)^2} \right], \quad (15)$$

with σ_T being the Thomson cross-section and n_e the number density of free electrons;

- for tensors, $\langle d(Q/\rho_\gamma)/dz \rangle$ is

$$\left\langle \frac{d(Q/\rho_\gamma)}{dz} \right\rangle_t = \frac{1.29}{48(1-R_\nu)} \times \int_0^{+\infty} d \log k \Delta_t^2(k) \frac{de^{-\Gamma\eta}}{dz}, \quad (16)$$

where $\Gamma = 32H(1-R_\nu)/15a\sigma_T n_e$, the damping of the gravitational wave amplitude due to photons, is approximately equal to 5.9 during radiation domination, *i.e.* when μ -distortions are generated. The factor of 1.29/2 arises from the average $\langle \mathcal{T}(x) \rangle$ of the transfer function $\mathcal{T}(k\eta)$ for tensor perturbations [82], once the effect of neutrino free-streaming [73, 83] is taken into account.

We note that in Eq. (16), the integral in $d \log k$ extends on all wavenumbers from $k = 0$ to $k = +\infty$: at long wavelengths the time derivative of the transfer function for the gravitational wave amplitude vanishes, so that no super-horizon heating occurs (we will not reproduce the calculations here, and refer to [73] for details). At small scales, however, there is an UV cutoff given by the photon mean free path $k_{\text{mfp}} = a\sigma_T n_e \approx 4.5 \times 10^{-7}(1+z)^2 \text{Mpc}^{-1}$, since for larger momenta photons stream quasi-freely and add little heating [30].

Taking into account the cutoff for the tensor case, one can obtain estimates for the contribution of scalar and tensor perturbations to the μ -distortion monopole

$$\langle \mu \rangle_s \approx 2.3 \times \frac{A_s}{n_s - 1} \left[\left(\frac{k}{k_\star} \right)^{n_s - 1} \right]_{k_d(z_{\mu,i})}^{k_d(z_{\mu,t})}, \quad (17a)$$

$$\langle \mu \rangle_t \approx 7.3 \times 10^{-6} \times \frac{rA_s}{n_t} \left[\left(\frac{k}{k_\star} \right)^{n_t} \right]_{k_{\text{mfp}}(z_{\mu,t})}^{k_{\text{mfp}}(z_{\mu,i})}. \quad (17b)$$

where $1/k_d(z)$ ($1/k_{\text{mfp}}(z)$) is the Silk damping scale (photon mean free path) at redshift z . Plugging in numerical

values, we get

$$\langle \mu \rangle_s \approx 2.3 \times \frac{A_s}{n_s - 1} \left[\left(\frac{k}{k_\star} \right)^{n_s - 1} \right]_{46 \text{ Mpc}^{-1}}^{1.1 \times 10^4 \text{ Mpc}^{-1}}, \quad (18a)$$

$$\langle \mu \rangle_t \approx 7.3 \times 10^{-6} \times \frac{rA_s}{n_t} \left[\left(\frac{k}{k_\star} \right)^{n_t} \right]_{1.1 \times 10^3 \text{ Mpc}^{-1}}^{1.8 \times 10^6 \text{ Mpc}^{-1}}. \quad (18b)$$

Tensors and scalar modes are not the only source of distortions: a third source is the so-called adiabatic cooling of photons [78, 84]. The difference in adiabatic indices of photons and baryons implies that, in the tight-coupling era, the baryonic matter must continuously extract energy from the CMB in order to establish $T_b \sim T_\gamma$. This cooling of the Planck spectrum would, in principle, lead to a Bose-Einstein condensation: however the time-scale for this to happen is quite long and no condensate is in reality possible. This effect can be described by a negative contribution to the overall $d(Q/\rho_\gamma)/dz$, given by [85]

$$\left\langle \frac{d(Q/\rho_\gamma)}{dz} \right\rangle_{\text{ac}} = \frac{3k_B[2n_H(z) + 3n_{\text{He}}(z)]}{2a_R(1+z)T_\gamma^3}, \quad (19)$$

where a_R is the radiation constant.

We take also this effect (which gives a $\langle \mu \rangle_{\text{ac}}$ of order -2.8×10^{-9}) into account in our analysis: the total μ -distortion is, then, the sum $\langle \mu \rangle = \langle \mu \rangle_s + \langle \mu \rangle_t + \langle \mu \rangle_{\text{ac}}$.

C. Pulsar timing + ground- and space-based interferometers

In this short section we briefly review the physics of interferometers and pulsar timing. We refer to [15] (and references therein) for a more detailed treatment, which is outside of the scope of this paper.

1. Pulsar timing

Pulsars are neutron stars formed during the supernova explosion of stars with 5 to 10 solar masses. Because of the great intrinsic stability of their pulsation periods, precision timing observations of pulsars (in particular, millisecond pulsars), can be used to detect GWs propagating in our Galaxy [86]: the reason is that the observed pulse frequencies will be modulated by gravitational waves passing between the pulsar and the Earth. This will give rise to a *timing residual*: the deviation of the observed pulse time of arrival from what is expected given our knowledge of the motion of the pulsar and the strict periodicity of the pulses. If one considers a gravitational wave propagating towards the Earth and traveling in the z -axis, the GW-induced timing residual of an observation at time t (calling t_0 the starting time of the

experiment) is given by [15]

$$\delta t^{\text{GW}} = \int_{t_0}^t dt \frac{1 - \cos \theta}{2} [\cos 2\psi h_+(t - s/c) + \sin 2\psi h_\times(t - s/c)], \quad (20)$$

where θ is the polar angle of the Earth-pulsar direction measured from the z -axis, ψ is a rotation in the plane orthogonal to the direction of propagation of the wave (in this case the (x, y) plane), corresponding to a choice of the axes to which the $+$ and \times polarization are referred, and $t - s/c$ is the time when the GW crossed the Earth-pulsar direction (with s being the distance along the path).

One can, therefore, relate the (variance of) these timing residuals to the energy density of the GW background. More precisely, EPTA will be sensitive to the integral of the spectrum $\Omega_{\text{GW}}(f)$ in a small interval of frequencies around the frequency f_{PTA} , which will be in the range $\sim 10^{-9} \text{ Hz} \div 10^{-7} \text{ Hz}$.

2. Ground- and space-based interferometers

The basis of present detectors is the effect of gravitational waves on the separation of adjacent masses on Earth or in space [87, 88]. GW strength is characterized by the change $2\Delta L/L$ in the separation of two masses a distance L apart. We consider a wave propagating in the z -direction, with *strain* $h_{\mu\nu}$ given by

$$h_{\mu\nu} = \begin{pmatrix} 0 & 0 & 0 & 0 \\ 0 & -h_+ & h_\times & 0 \\ 0 & h_\times & h_+ & 0 \\ 0 & 0 & 0 & 0 \end{pmatrix}, \quad (21)$$

and place two masses at the origin and at $x = L$. We can measure the distance between the two masses by sending a laser beam from the source at $x = 0$ to $x = L$ and back, and measure the phase of the returned beam relative to that of the source. In the presence of a gravitational wave, the ‘‘round-trip (rt) phase’’ $\Phi(t_{\text{rt}})$ is

$$\Phi_x(t_{\text{rt}}) = 2 \frac{2\pi\nu}{c} \int_0^L dx \sqrt{g_{xx}} \approx 2 \left(1 - \frac{h_+}{2}\right) \frac{2\pi L}{\lambda}, \quad (22)$$

for ‘‘plus’’ oriented wave with a period much longer than the round-trip light travel time. With an analogous set-up along the y -axis, instead, one gets

$$\Phi_y(t_{\text{rt}}) \approx 2 \left(1 + \frac{h_+}{2}\right) \frac{2\pi L}{\lambda}. \quad (23)$$

The difference in phase shift $\Delta\Phi = \Phi_y(t_{\text{rt}}) - \Phi_x(t_{\text{rt}})$ between the two arms will be proportional, then, to the gravitational wave amplitude h_+ . Considering averages of the squared difference in phase shift, direct detection experiments are able to probe the spectrum of a stochastic background of gravitational waves.

III. METHOD

A. Monte Carlo method and datasets

We perform a Monte Carlo Markov Chain (MCMC) analysis, using the publicly available code `cosmomc` [89, 90]. We vary the six standard Λ CDM cosmological parameters, namely the baryon density $\Omega_b h^2$, the cold dark matter density $\Omega_c h^2$, the sound horizon angular scale θ , the reionization optical depth τ , the amplitude $\log(10^{10} A_s)$ and spectral index n_s of the primordial spectrum of scalar perturbations. We add to these the tensor-to-scalar ratio r and the tensor spectral index n_t . Unless otherwise stated, we normalize the inflationary parameters to the pivot wavelength $k = 0.01 \text{ Mpc}^{-1}$, roughly corresponding to $\ell \simeq 150$, using the approximate formula $\ell \sim 1.35 \times 10^4 (k/\text{Mpc}^{-1})$. This is where the data published by the BKP collaboration are most sensitive and it is close to the decorrelation scale between the tensor amplitude and slope for Planck and BKP joint constraints [13].

Our reference dataset is based on CMB temperature and polarization anisotropies. We analyze the BB power spectrum as measured by the BKP collaboration (first five bandpowers) [11], in combination with the temperature and polarization *Planck* likelihood [10]. More precisely, we make use of the TT , TE , EE high- ℓ likelihood together with the TQU pixel-based low- ℓ likelihood. We also compare the BKP BB power spectrum to the recently released BICEP2/*Keck Array* polarization data (BK14, hereafter) [12]. Note that, when using these datasets, we perform the analysis both with and without $N_{\text{eff}}^{\text{GW}}$. The second case could seem unrealistic: in fact, if GWs are present, they will surely contribute to the number of effective radiation d.o.f. However, it is possible to have scenarios where the contribution of neutrinos to N_{eff} is lower than 3.046 [91–93]. For this reason instead of referring to a specific non-standard model for computing the contribution of neutrinos to N_{eff} and subsequently add the $N_{\text{eff}}^{\text{GW}}$ contribution, we follow a more generic approach and we assume a total value of relativistic degrees of freedom of 3.046 (in agreement with current cosmological constraints) as the final sum of the two contributions.

We will consider, then, the following extensions to our reference dataset:

- **BAO and Deuterium.** We use baryon acoustic oscillations (BAO) to break geometrical degeneracies, as reported in [94]: the surveys included are 6dFGS [95], SDSS-MGS [96], BOSS LOWZ [97] and CMASS-DR11 [97]. We use primordial Deuterium abundance measurements [42] to constrain the relativistic number of degrees of freedom, assuming standard BBN. We do not use primordial helium measurements, since they are less constraining: this is due to the uncertainty in the neutron lifetime, which affects the computation of the helium abundance that will be then compared to

observations (for a recent discussion about the effect of this uncertainty on cosmological parameter estimation, we refer to [98]). When used in combination with CMB data, we will denote this joint dataset by EXT;

- FIRAS limits on deviations of the CMB from a black-body spectrum, $\mu = (1 \pm 4) \times 10^{-5}$ (at 68% CL) [28];
- LIGO-Virgo limit on $\Omega_{\text{GW}}(f)$ for frequencies in the band 41.5 Hz–169.25 Hz coming from the LIGO and Virgo joint analysis [99], *i.e.* $\Omega_{\text{GW}}(f) \leq 5.6 \times 10^{-6}$ (95% CL). We note that the scales at which LIGO-Virgo is sensitive are likely dominated by astrophysical GW backgrounds (such as, *e.g.*, gravitational waves from binary mergers or rotating neutron stars): for this reason the limits that we will obtain on n_t in this case must be regarded as conservative;
- pulsar constraints on a stochastic relic GW background at $f = 2.8 \times 10^{-9}$ Hz obtained by EPTA in [100], *i.e.* $\Omega_{\text{GW}}(f) \leq 1.2 \times 10^{-9}$ (95% CL).

B. Simulated datasets for forecasts

For our forecasts we generate simulated datasets following the approach described in [101] (see also Sec. VIB). Regarding the presence of foregrounds (like dust and synchrotron emission), we assume that these can be removed after being characterized by the high- and low-frequency channels of COre (i.e. $\nu \gtrsim 100$ GHz and $\nu \lesssim 230$ GHz), where the CMB is subdominant. We also assume that uncertainties due to foreground removal are smaller than instrumental noise (which we take as white and isotropic), and that beam uncertainties are negligible. We account for the impossibility of observing the full sky simply by reducing the degrees of freedom at each multipole ℓ with the sky fraction f_{sky} (see Sec. VIB), and ignoring the induced correlations between different ℓ . Our fiducial model is described in Tab. I, while the specifics used for the COre-like mission are listed in Tab. II.

In some cases, we consider also the upgraded version of current interferometer experiments, in combination with COre simulated data. In particular, we focus our attention on AdvLIGO [66] (which we refer to as aLIGO in our plots), that will be able to reach a sensitivity of 10^{-9} on $\Omega_{\text{GW}}(f)$ at $f = 100$ Hz.

We also compare the forecasts from COre alone with those from the combination *Planck* + BKP + AdvLIGO and *Planck* + BK14 + AdvLIGO: since a COre-like mission (*i.e.* COre++, see [102]) is still in proposal stage, it is worth to investigate how limits on tensor parameters will improve thanks only to advancements in GW direct detection.

Parameter	Fiducial value
$\Omega_b h^2$	0.02225
$\Omega_c h^2$	0.1198
$100\theta_{\text{MC}}$	1.04077
τ	0.079
n_s	0.9645
$\log(10^{10} A_s)$	3.145
H_0	67.77
z_{eq}	3394

TABLE I. Fiducial cosmological parameters used for the COre forecasts: the fiducials for the tensor parameters r and n_t are specified in the main text.

channel (GHz)	FWHM (arcmin)	$w^{-1/2} - T$ ($\mu\text{K} \cdot \text{arcmin}$)	$w^{-1/2} - Q, U$ ($\mu\text{K} \cdot \text{arcmin}$)
105	10	2.68	4.63
135	7.8	2.63	4.55
165	6.4	2.67	4.61
195	5.4	2.63	4.54
225	4.7	2.64	4.57

TABLE II. Temperature and polarization noise (in $\mu\text{K} \cdot \text{arcmin}$) and beam (FWHM in arcmin) specifications of the COre experiment, from [65]. We suppose that the ten additional frequency channels (from 45 GHz to 795 GHz) are used for foreground cleaning. The fraction of sky covered is $f_{\text{sky}} = 0.8$.

C. Delensing

Tensor modes are not the only source of B -mode polarization: gravitational lensing, in fact, generates a non-Gaussian B -mode signal [103]. While interesting in its own right (see [104] for a review), it acts as another source of foregrounds when the goal is studying primordial tensor modes. However, if the lensing potential is reconstructed on small scales, one can remove the lensing contribution to the CMB B -mode spectrum at large scales, where the contribution from tensors dominates [105–108].

In the recent work [70] (more precisely, we refer to Fig. 4 – left panel) it is shown that, for an experiment with a noise level of order $\sim 1 \mu\text{K} \cdot \text{arcmin}$ post component separation, one can bring the power of lensing B -modes down to 10% of their original value (see Fig. 2). Since we expect that COre could reach these noise levels after component separation has been carried out, we implement a 10% delensing in our forecasts following [109], *i.e.* by rescaling the lensing B -mode angular spectrum C_ℓ^{lens} of a factor of 0.1. This removal of lensing B -modes

allows us to gain sensitivity to the scale dependence of Δ_t^2 on a wider range of multipoles. In Fig. 2 we see that if the C_ℓ^{lens} are reduced to 10% in power, for $r = 0.1$ there are ~ 100 more multipoles available before the noise becomes larger than the signal. For lower values of the tensor-to-scalar ratio the gain would be even larger [110].

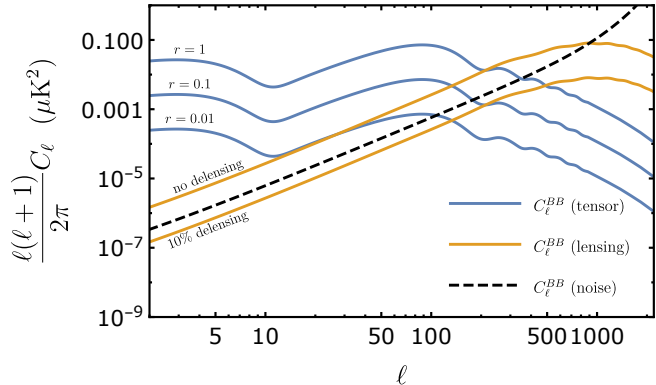


FIG. 2. Tensor and lensing B -modes, together with noise bias for the CORe experiment. The blue spectra correspond $r = 1, 0.1, 0.01$ and $n_t = 0$, while the orange ones are the lensing B -mode spectrum with and without a rescaling by a factor of 0.1. We see that in the case of a 10% delensing the C_ℓ^{lens} go completely below noise level.

IV. RESULTS

A. Current data

We begin this section with a discussion about priors. In the absence of primordial GWs detection, the bounds on the tensor tilt will be prior dependent: while taking a flat prior around $n_t = 0$ is strongly motivated by scale invariance, there is no equivalently strong guidance on the prior range: in fact the effect of a very blue tilt could always be cancelled by a very small tensor-to-scalar ratio. For this reason, the limits we put on n_t depend on which sampling of r we use for our MCMC exploration of parameter space: we have used in our analysis a linear prior on r , with $r > 0.001$ [111]. Had we chosen, *e.g.*, a logarithmic prior on r , the tails of the two-dimensional contours depicted in Figs. 3, 4 would have extended on a wider range on the n_t -axis, and the marginalized constraints on the tilt would have degraded: the more one samples regions at low r , the less tight the bounds on the tilt will be. This is a very important point, that must be kept in mind when interpreting Figs. 3, 4 and Tabs. III, IV.

Turning to the actual results, the first thing we notice from the left panel of Fig. 3 is that the posteriors for n_t favor a blue tilt, when $N_{\text{eff}}^{\text{GW}}$ is turned off and no additional observables besides CMB anisotropies are considered. This is due to the fact that we normalize our spectra at a pivot of 0.01 Mpc^{-1} . In fact, in order to

be consistent with the low tensor power at large scales, where the constraints from the *Planck* data come from, a blue tilt is needed [112].

When we add the information from spectral distortions, pulsar timing or GW direct detection, instead, we find that the upper limits for the tilt decrease, in agreement with the fact that a too large n_t would lead to a large and detectable tensor signal at small scales. Moreover, there is an almost horizontal cut in the two-dimensional posteriors for r and n_t : the reason is that the dependence of these three observables on the tilt is exponential, and this causes the posterior probability density function to be very steep in the n_t direction. The left panel of Fig. 3 shows that the most constraining dataset is *Planck* + BKP + LIGO-Virgo, followed by *Planck* + BKP + pulsar and *Planck* + BKP + FIRAS.

This hierarchy is expected since the tensor and scalar contributions for spectral distortions are degenerate (as one can see from Sec. II B), and Eqs. (18) show that the scalar contribution $\langle \mu \rangle_s$ dominates over the tensor one unless n_t is very large. Regarding the *Planck* + BKP + pulsar and *Planck* + BKP + LIGO-Virgo datasets we could have expected to obtain better constraints with pulsar timing than with direct GW measurements, since the former put more stringent upper limits on Ω_{GW} . The reason why this does not happen is that the frequency range where pulsar timing operates is closer to the horizon size at recombination than LIGO-Virgo frequencies, therefore giving a weaker lever arm to estimate the scale dependence of the primordial tensor spectrum.

Our best bounds on the tensor parameters, obtained using the *Planck* + BKP + LIGO-Virgo dataset, are $r < 0.085$ and $n_t = 0.04_{-0.85}^{+0.61}$ (both at 95% CL).

Another thing that we notice is the following: since the low tensor power at large scales cannot be anymore accommodated by having a blue tensor tilt, the upper limits on the tensor-to-scalar ratio decrease as those on n_t become tighter. This does not happen, however, for the *Planck* + BKP + FIRAS dataset: the reason is that the best-fit of *Planck* + BKP is excluded by the combination *Planck* + BKP + FIRAS, so regions of parameter space that were before forbidden at more than 2σ become again compatible with data at 95% CL. The same argument applies also to *Planck* + BKP + pulsar and *Planck* + BKP + LIGO-Virgo: in that case, however, the constraints on the tilt derived from Ω_{GW} are strong enough that r must be brought down in order to have consistency with the *Planck* + BKP bounds on the large-scale tensor power.

The left panel of Fig. 4 and Tab. IV show that switching from BKP to BK14 polarization data has mainly the effect of tightening the bounds on the tensor-to-scalar ratio, while those for n_t are practically unaffected. Given that the BK14 dataset puts more precise bounds on the BB power spectrum, one could expect to obtain also strongest constraints on the tensor tilt. However, since BK14 spectra prefer values of r lower than BKP ones, the gain from the higher experimental accuracy is cancelled

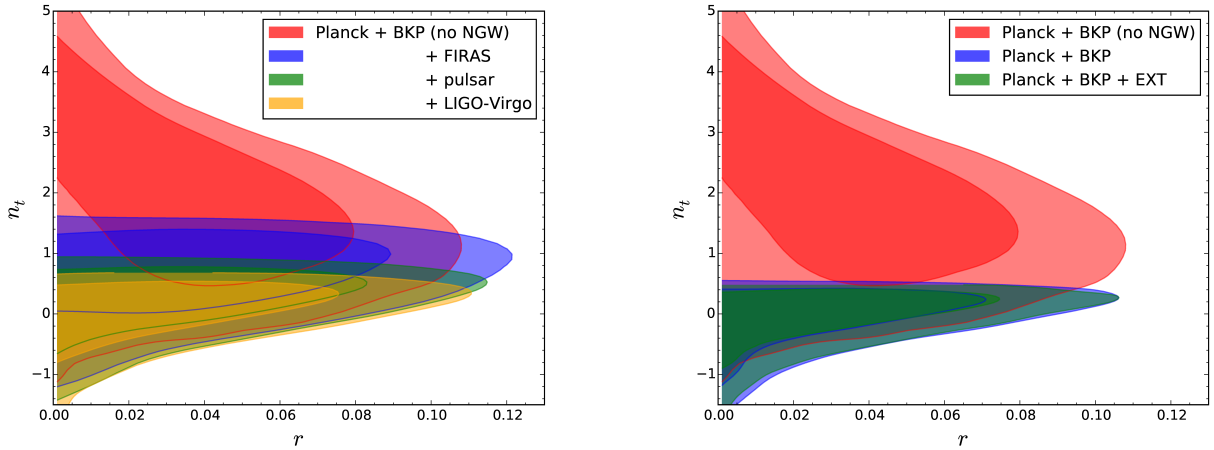


FIG. 3. Two-dimensional posterior distributions for r and n_t : the contours in the left (right) panel are obtained without (with) the inclusion of $N_{\text{eff}}^{\text{GW}}$. In both panels the red contour is the result for the “vanilla” $\Lambda\text{CDM} + r + n_t$ model, using the *Planck* + BKP dataset. The corresponding 95% CL results for r and n_t are reported in Tab. III.

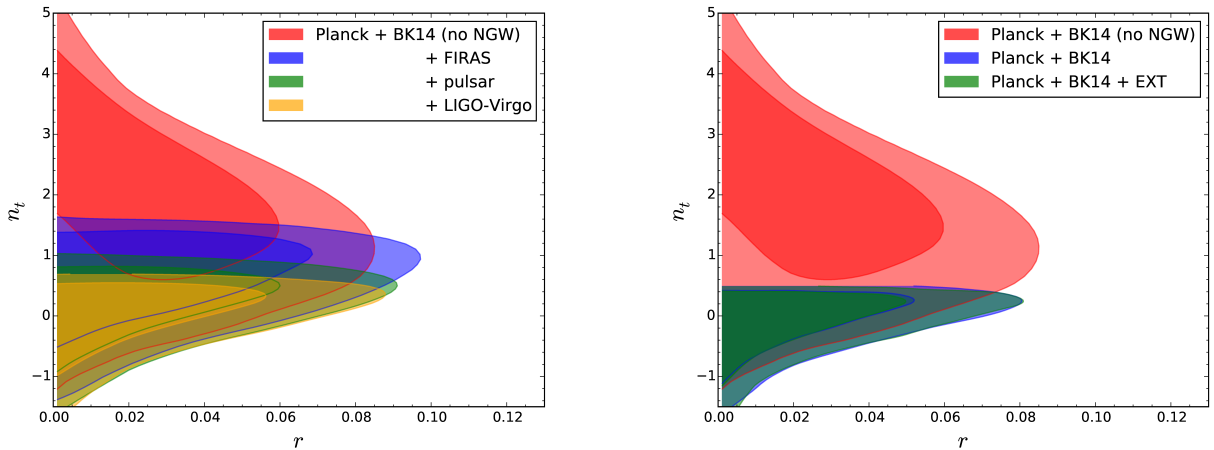


FIG. 4. Two-dimensional posterior distributions for r and n_t , using BK14 polarization data: the contours in the left (right) panel are obtained without (with) the inclusion of $N_{\text{eff}}^{\text{GW}}$. The corresponding 95% CL results for r and n_t are reported in Tab. IV.

by the lost sensitivity of the angular spectra to variations in n_t .

Similarly to the previous case, the best bounds on tensor parameters ($r < 0.067$, $n_t = 0.00^{+0.68}_{-0.91}$, both at 95% CL) are obtained by the combination of CMB anisotropies and direct detection experiments.

When we add the contribution $N_{\text{eff}}^{\text{GW}}$ to the effective number of degrees of freedom N_{eff} , Tab. III shows that we obtain more stringent constraints on r and n_t , while we see from the right panel of Fig. 3 that the steep slope of the posterior in the n_t direction is reproduced (recall Eqs. (12)). In particular we see that in this case, even if we are using “just CMB information” (*i.e.* the effect of N_{eff} on CMB anisotropies only), we reach a constraining power comparable to or even better than CMB com-

bined with GW direct detection experiments. Of course, by adding external astrophysical datasets (as BAO and primordial Deuterium abundance) we obtain even tighter bounds. Our best limits, obtained using *Planck* + BKP + EXT, are $r < 0.080$ and $n_t = -0.05^{+0.57}_{-0.80}$, both at 95% CL.

Also in this case, adding the BK14 dataset leads to better constraints on r : we see from Tab. IV that considering the *Planck* + BK14 + EXT dataset we reach $r < 0.061$ (95% CL).

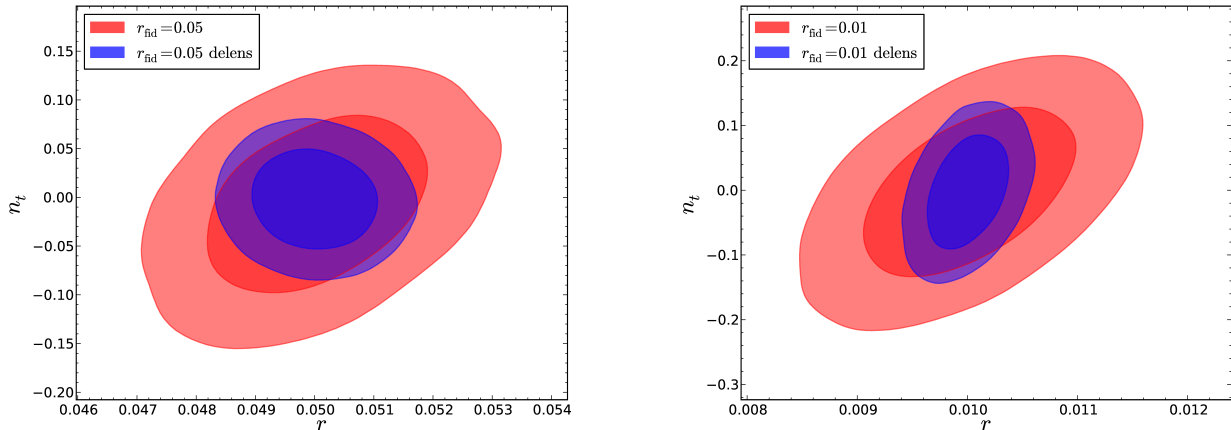


FIG. 5. Forecasts for r and n_t with two different fiducials: $r = 0.05$ (left panel) and $r = 0.01$ (right panel). In both cases the inflationary consistency relation $n_t = -r/8$ has been assumed. The corresponding 95% CL limits for r and n_t are reported in Tab. V.

Dataset	r	n_t
<i>Planck</i> + BKP	< 0.089	$1.7^{+2.2}_{-2.0}$
<i>Planck</i> + BKP + FIRAS	< 0.098	$0.65^{+0.86}_{-1.1}$
<i>Planck</i> + BKP + pulsar	< 0.088	$0.20^{+0.69}_{-0.96}$
<i>Planck</i> + BKP + LIGO-Virgo	< 0.085	$0.04^{+0.61}_{-0.85}$
<i>Planck</i> + BKP, with $N_{\text{eff}}^{\text{GW}}$	< 0.082	$-0.05^{+0.58}_{-0.87}$
<i>Planck</i> + BKP + EXT, with $N_{\text{eff}}^{\text{GW}}$	< 0.080	$-0.05^{+0.57}_{-0.80}$
<i>Planck</i> + BKP + aLIGO	< 0.078	$-0.09^{+0.54}_{-0.78}$

TABLE III. Constraints at 95% CL on the tensor-to-scalar ratio r and the tensor spectral index n_t for the listed datasets: the first four results are obtained without considering the GW contribution to N_{eff} . For a detailed description of the datasets used in the analysis see Sec. III A. For the *Planck* + BKP + aLIGO forecast we assumed no detection for AdvLIGO.

Dataset	r	n_t
<i>Planck</i> + BK14	< 0.067	$1.8^{+2.0}_{-2.1}$
<i>Planck</i> + BK14 + FIRAS	< 0.078	$0.63^{+0.89}_{-1.16}$
<i>Planck</i> + BK14 + pulsar	< 0.070	$0.17^{+0.75}_{-1.03}$
<i>Planck</i> + BK14 + LIGO-Virgo	< 0.067	$0.00^{+0.68}_{-0.91}$
<i>Planck</i> + BK14, with $N_{\text{eff}}^{\text{GW}}$	< 0.061	$-0.12^{+0.65}_{-0.84}$
<i>Planck</i> + BK14 + EXT, with $N_{\text{eff}}^{\text{GW}}$	< 0.061	$-0.10^{+0.63}_{-0.88}$
<i>Planck</i> + BK14 + aLIGO	< 0.060	$-0.16^{+0.63}_{-0.88}$

TABLE IV. Same as Tab. III, but considering BK14 polarization data in addition to *Planck* power spectra. For a detailed description of the datasets we refer to Sec. III A. As in table III for AdvLIGO we assumed no detection of primordial GWs.

B. Forecasts

The results of our forecasts are reported in Figs. 5, 6 and Tabs. V, VI. For our first forecast we assume no detection of Ω_{GW} in the future interferometer experiment AdvLIGO. The datasets we consider are the combination of current CMB measurements (*Planck* + BKP and *Planck* + BK14) and AdvLIGO experiment. Comparing the results obtained with the current data alone and in combination with AdvLIGO (Tabs. III, IV), we see that the constraining power of the next generation of direct detection experiments will be similar to what can be obtained by CMB experiments alone when the contribution $N_{\text{eff}}^{\text{GW}}$ to N_{eff} is included.

We have then considered two fiducial cosmologies, one with $r = 0.05$ and one with $r = 0.01$: in both cases we have taken a fiducial value of the tilt given by $r = -n_t/8$. The two-dimensional posteriors in the $r - n_t$ plane (Fig. 5) confirm what has been said in Sec. III C: when lensing B -modes are removed, one is able to disentangle the effects of r and n_t on the tensor B -mode spectrum (since more scales become available and one can distinguish a tilted spectrum from one that is simply rescaled by r).

Tab. V shows that CORe will be able to measure $r = 0.01$ with a relative uncertainty of order 3×10^{-2} (10^{-2} with 10% delensing). On the other hand it also shows that, even when delensing is considered, CORe will not be able to probe the inflationary consistency relation with high enough accuracy to pin down single-field slow-roll inflation as the mechanism for the generation of primordial perturbations: in fact we see that σ_{n_t}/n_t will be very large, of order 10 for the $r = 0.05$ fiducial, and of order 100 for the $r = 0.01$ one. This tells us that the range of scales probed by the CMB will not be sufficient to test the scale dependence of the tensor spectrum in the next future: combining CMB measurements with direct

detection experiments will be necessary.

Finally, we assume the best-fit from the *Planck* + BKP + LIGO-Virgo dataset, *i.e.* $r = 0.045$, $n_t = 0.35$, as our fiducial model [113]: the simulated datasets used are *Planck* + BKP + AdvLIGO, COre, COre with 10% delensing and COre + AdvLIGO (without delensing). We have chosen a ground-based direct detection experiment as additional observable because the lever arm with the scales probed by CMB anisotropies is the strongest available (see Fig. 1). Besides, since AdvLIGO will put constraints directly on Ω_{GW} , it will be less dependent on the underlying cosmological models than observables like μ -distortions.

The results are reported in Fig. 6 and Tab. VI. The first thing to notice is that *Planck* + BKP + AdvLIGO will give a detection of the tensor tilt, while at 95% CL we will still have only upper bounds on r . This is due to the fact that AdvLIGO will actually be able to detect the stochastic background of GWs for these fiducial values of the tensor parameters: however, the tensor power at CMB scales is still too low for *Planck* + BKP to have a detection of r .

Comparing the forecasts from COre [114] with those from the combination *Planck* + BKP + AdvLIGO, we see that COre + 10% delensing will result in better constraints on the tensor parameters than what can be obtained from the evolution of LIGO to AdvLIGO. This is worthy of notice also because the constraints from COre, that will be derived using data from a single experiment (and then with better control of systematics), will be more reliable.

We also see that combining COre with the improved version of LIGO will allow to obtain tighter constraints on the tensor tilt than those coming from COre alone, even if a 10% delensing is taken into account. More precisely, there is roughly a factor of 5 improvement of σ_{n_t} . On the other hand, we see that the bounds on the tensor-to-scalar ratio are basically unaffected if we add AdvLIGO to the forecast.

We conclude this section with a brief discussion about inflationary models: more precisely about the possibility of having a model with r and n_t equal to the best-fit from the *Planck* + BKP + LIGO-Virgo dataset. One of the main features of single-field slow-roll is the presence of the so-called consistency relation: it relates the tilt of the primordial tensor spectrum to the Hubble slow-roll parameter during inflation, $\epsilon_H \equiv -\dot{H}/H^2$, by

$$n_t = -2\epsilon_H . \quad (24)$$

Single-field slow-roll models do not violate the Null Energy Condition (NEC) $\dot{H} < 0$, thus predicting a red tensor spectral index $n_t < 0$. It is possible, however, to construct models that violate the NEC and lead to a blue n_t without incurring in instabilities, like G-inflation [115] and Ghost inflation [116]. While in Ghost inflation gravitational waves are predicted to be completely unobservable, G-inflation can give $r = \mathcal{O}(10^{-2})$, $n_t = \mathcal{O}(10^{-1})$: however, it also predicts that the scalar and tensor modes

tilt towards the same direction [117], and a blue $n_s > 1$ is well excluded by current data (see Tab. I).

If these inflationary models are hard-pressed to accommodate such values of the tensor tilt and the tensor-to-scalar ratio, there are other scenarios that can predict a blue n_t while keeping the scalar sector in accord with observations:

- particle or string sources produced during inflation can generate blue tensor modes consistent with the constraints from scalar fluctuations [117, 118];
- gauge field production in axion inflation [119, 120] can also lead to blue tensor spectra;
- it is possible to violate the tensor consistency relation also with higher-curvature corrections to the gravitational effective action (coming, *e.g.*, from string theory) [121, 122]. In these cases, a time-dependent speed of sound of tensor perturbations changes the consistency relation to

$$n_t = -2\epsilon_H + \mathcal{B}\sqrt{\epsilon_H} . \quad (25)$$

In [122] the authors show that it is possible to make the factor \mathcal{B} positive and of order one, and therefore have $n_t \lesssim \mathcal{O}(10^{-1})$.

We refer to Sec. VIC for a more detailed discussion about these models.

	r	n_t
fiducial	0.05	$-r/8 = -0.00625$
COre	0.0500 ± 0.0012	$-0.0072^{+0.1108}_{-0.1143}$
COre, delens.	0.05000 ± 0.00066	$-0.0023^{+0.0632}_{-0.0640}$
fiducial	0.01	$-r/8 = -0.00125$
COre	0.01001 ± 0.00061	$-0.0024^{+0.1597}_{-0.1637}$
COre, delens.	0.01000 ± 0.00024	$-0.0019^{+0.1074}_{-0.1088}$

TABLE V. Future constraints at 95% CL on the tensor-to-scalar ratio r and the tensor spectral index n_t from a COre-like mission (with and without 10% delensing). In none of this cases the contribution of $N_{\text{eff}}^{\text{GW}}$ to N_{eff} has been included.

V. CONCLUSIONS

In this paper we investigate the constraints on the primordial tensor power spectrum, assuming that it is described by a power law with tilt n_t and tensor-to-scalar ratio r , normalized at a pivot scale $k = 0.01 \text{ Mpc}^{-1}$. We compare the bounds from Cosmic Microwave Background temperature and polarization anisotropies alone with those obtained by adding to the analysis CMB spectral distortions (FIRAS), pulsar timing (European Pulsar Timing Array), and direct detection experiments such as

	r	n_t
fiducial	0.045	0.35
$P + \text{BKP} + \text{aLIGO}$	< 0.095	0.354 ± 0.020
COre	0.0450 ± 0.0011	0.348 ± 0.061
COre, delens.	0.04500 ± 0.00060	0.350 ± 0.029
COre + aLIGO	0.0450 ± 0.0010	0.3483 ± 0.0053

TABLE VI. 95%CL constraints on r and n_t from *Planck* + BKP + AdvLIGO (denoted by $P + \text{BKP} + \text{aLIGO}$), COre alone (with and without delensing), and from COre + AdvLIGO, for a fiducial equal to the best-fit of the *Planck* + BKP + LIGO-Virgo analysis of Sec. IV A (*i.e.* $r = 0.045$, $n_t = 0.35$).

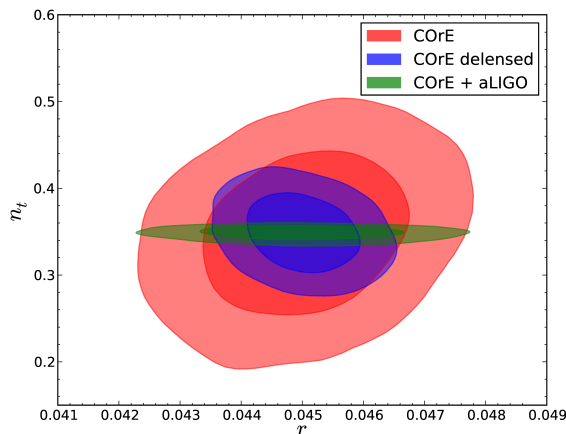


FIG. 6. Two-dimensional posterior distributions for r and n_t from COre (with and without delensing) and COre + AdvLIGO. The fiducial values are fixed to the best-fit of the *Planck* + BKP + LIGO-Virgo analysis (*i.e.* $r = 0.045$ and $n_t = 0.35$), and the 95% CL constraints are reported in Tab. VI. We preferred to not include the contours from *Planck* + BKP + AdvLIGO (which extend outside of the frame of this plot) to better show the improvement from COre to COre + AdvLIGO.

LIGO-Virgo: we find that the gradually stronger lever arm allows to increase the sensitivity from $r < 0.089$, $n_t = 1.7^{+2.2}_{-2.0}$ (*Planck* + BKP, 95% CL) to $r < 0.085$, $n_t = 0.04^{+0.61}_{-0.85}$ (*Planck* + BKP + LIGO-Virgo, 95% CL).

Taking into account the contribution of gravitational waves to the effective number of relativistic degrees of freedom $N_{\text{eff}} = 3.046 + N_{\text{eff}}^{\text{GW}}$, and the subsequent effect of an increased radiation energy density on CMB angular spectra and primordial abundances, the bounds on r and n_t further improve, arriving at $r < 0.081$, $n_t = -0.05^{+0.58}_{-0.84}$ (*Planck* + BKP, 95% CL). These limits on the tensor parameters are stronger than what results from the *Planck* + BKP + LIGO-Virgo dataset: it must be kept in mind, however, that one must make an explicit assumption about the scale (k_{UV}) beyond which primordial GWs are not produced, in order to express $N_{\text{eff}}^{\text{GW}}$ in terms of the primordial tensor spectrum. Even by choos-

ing this cutoff to be the scale crossing the horizon at the end of inflation, there is still freedom to vary it due to the uncertainties on the reheating mechanism. In this paper we make the assumption $k_{\text{UV}} = 10^{23} \text{ Mpc}^{-1}$, which corresponds to having an instantaneous transition to radiation dominance after inflation ends: this is a conservative choice with respect to other works (which choose, *e.g.*, k_{UV} equal to the inverse Planck length), but can lead to an overestimation of $N_{\text{eff}}^{\text{GW}}$ in the case of non-instantaneous reheating.

If the recently released 95 GHz data from *Keck Array* are added to the analysis, we find that, while the constraints on the tilt do not get appreciably better, the bounds on the tensor-to-scalar ratio are improved up to $\sim 20\%$: for the *Planck* + BK14 + LIGO-Virgo dataset we find $r < 0.067$ (95% CL), while the *Planck* + BK14 + EXT dataset gives $r < 0.061$ (95% CL).

We show that, even with the $10\times$ improvement in sensitivity of the upcoming AdvLIGO, the constraints from CMB anisotropies alone will still be stronger than those coming from interferometers, if the contribution $N_{\text{eff}}^{\text{GW}}$ to N_{eff} is considered.

In the absence of detection, the posterior probability distribution for the tensor tilt will depend strongly on the prior: for this reason we have also investigated how a future COre-like CMB mission will be able to constrain r and n_t , in the case of fiducial cosmologies with r of order 10^{-2} and $n_t = -r/8$ (as per inflationary consistency relation). This value of r has been chosen because it is high enough to be in the reach of not-so-distant experiments like AdvACT.

We find that COre will measure r with a σ_r/r of order 10^{-2} , while the relative uncertainty on n_t will be much larger (of order 10 for the $r = 0.05$ fiducial and of order 100 for the $r = 0.01$ one). Subtracting lensing B -modes to 10% of their power (an feasible goal for experiments where noise can be brought down to $\sim 1 \mu\text{K} \cdot \text{arcmin}$ after component separation) does little to improve these constraints: however, delensing allows a “CMB-only” mission to become competitive with the combination of *Planck* + BKP (BK14) and the upgrade of LIGO, *i.e.* AdvLIGO.

Finally, we consider a fiducial model where r and n_t are those preferred by the *Planck* + BKP + LIGO-Virgo dataset. We compare the forecasts for COre with those for COre combined with AdvLIGO, and we find that adding AdvLIGO will result in a order 5 improvement on σ_{n_t} with respect to constraints from CMB anisotropies alone, even if we assume that a 10% delensing will be carried out.

We conclude the summary of our results briefly discussing the forecasts for PIXIE [63]. PIXIE will provide both photometry and spectrometry: therefore it will allow to combine temperature and polarization constraints with those from spectral distortions, while reducing the risk of systematics caused by the combination of datasets from different experiments. However, we have found that adding the bounds on μ -distortions will not lead to a de-

cisive improvement: the reason is that $\langle \mu \rangle$ is dominated by the contribution of scalar perturbations for the values of r and n_t allowed by the constraints from photometry alone. So, since the main constraining power will come from temperature and polarization anisotropies, we preferred to focus on COrE, whose primary goal will be to improve sensitivity to these two observables.

An interesting development of this work would be to consider upcoming experiments that will measure the expansion history more accurately, and reduce the error on the number N_{eff} of massless degrees of freedom (see for example [123]: Fig. 2 – right panel). In fact, a non-detection of extra radiation would impose strong constraints on the contribution of GWs to N_{eff} , and then to the tensor parameters r and n_t [124].

Another possible development would be to consider a different parametrization of the primordial tensor power spectrum. The assumption of having a power law spectrum down to the scales probed by direct detection experiments is very strong: in the inflationary theory, the more one approaches the end of inflation, the more power spectra will deviate by the slow-roll result [125]. Therefore, while writing $\Delta_t^2(k)$ as a power law is still acceptable when one considers a small range of scales (like the one probed by the CMB), the inclusion of observables which probe scales up to $k \approx 10^{19} \text{ Mpc}^{-1}$ can become at odds with this simple parametrization. One possibility to avoid this problem would be to write $\Delta_t^2(k)$ as a step function, and take its k -bins to be those shown in Fig. 1.

While we were completing this work, [126] and [127] appeared to the arXiv. In the first paper, the authors study how the search for the primordial B -mode signal will be affected by any imperfect modeling of foregrounds, focusing on their impact on the tensor-to-scalar ratio. In this work we have assumed that foregrounds can be characterized well enough to be taken below instrumental noise: we will investigate the effect of foreground modeling for forecasts on the tensor tilt in a future work. In the second paper, the authors also combine bounds on the tensor tilt coming from CMB measurements (direct and indirect, through the effect of GWs on N_{eff}), together with pulsar timing and direct detection experiments: we find that, when direct comparison is possible, the results of our works overlap. We also note that [127] takes an alternative approach regarding the prior-dependence of the bounds in the absence of detection: they choose a logarithmic prior on the tensor-to-scalar ratio.

ACKNOWLEDGMENTS

We would like to thank Daniel Baumann, Josquin Errard, Rishi Khatri, Massimiliano Lattanzi and Enrico Pajer for useful discussions and comments on the draft. We would like to thank Antony Lewis for the use of the numerical codes `cosmomc` and `camb`. We acknowledge support by the research grant Theoretical Astroparticle Physics number 2012CPPYP7 under the program PRIN 2012

funded by MIUR and by TASP, iniziativa specifica INFN.

VI. APPENDIX

A. Horizon size at the end of inflation

One starts from the following identity for the number N_* of e-folds of inflation after a scale k_* has left the horizon (see [128] for a derivation)

$$\begin{aligned} N_* &\equiv \log \frac{a_{\text{end}}}{a_*} \\ &= -\log \frac{k_*}{H_0} + \log \frac{H_*}{H_0} + \log \frac{a_{\text{end}}}{a_{\text{reh}}} + \log \frac{a_{\text{reh}}}{a_0}, \end{aligned} \quad (26)$$

where t_{reh} marks the transition to radiation dominance. Then, by taking $k_* = k_{\text{end}}$ (*i.e.* $N_* = 0$) and making the standard assumption of reheating being a period of matter domination, one can show that

$$\begin{aligned} \frac{k_{\text{end}}}{\text{Mpc}^{-1}} &= T_{\text{CMB}} \exp \left[\log \sqrt[3]{\beta} - \log \sqrt{3} + \log \sqrt[3]{\alpha^2} \right. \\ &\quad \left. + \log \sqrt[3]{\frac{\pi^2}{45} g_*(T_{\text{CMB}})} \right], \end{aligned} \quad (27)$$

where $E_{\text{end}} = (\alpha M_{\text{P}})^4$ and $T_{\text{reh}} = \beta M_{\text{P}}$ are the energy density at the end of inflation and the temperature of the universe at the beginning of radiation dominance, respectively.

Now: plugging in numerical values for the CMB temperature at the present time ($T_{\text{CMB}} \approx 2.7 \text{ K}$), and assuming to have instant reheating ($\alpha = \beta$) at the GUT scale $E_{\text{end}} \approx 10^{16} \text{ GeV}$ ($\alpha \approx 10^{-2}$), the result is $k_{\text{end}} \approx 2 \times 10^{23} \text{ Mpc}^{-1}$ as reported in the main text.

B. Forecasting method

To describe the forecasting method used throughout this paper, we focus for simplicity on a single anisotropy spectrum of the Cosmic Microwave Background: the generalization to the full T , E , B spectra is straightforward [129]. We start from the expression for the likelihood of a full-sky experiment, *i.e.* (disregarding factors of 2π)

$$\mathcal{L} = \frac{1}{\sqrt{\det(C_S + C_N)}} e^{-\frac{1}{2} \Delta^T \cdot (C_S + C_N)^{-1} \cdot \Delta}, \quad (28)$$

with data points $\Delta_{\ell m}^i = s_{\ell m}^i + n_{\ell m}^i$ at each pixel (labelled by ℓm since we work in harmonic space) and each frequency channel i . The signal $s_{\ell m}^i$ is given by $\hat{W}_c^i \hat{a}_{\ell m}^c$, where the $\hat{a}_{\ell m}^c$ are the harmonic coefficients of the (beam-smoothed) temperature anisotropy for each component c (*i.e.* CMB + foregrounds such as dust, synchrotron, etc.), and the shape vector \hat{W}_c^i provides the frequency dependence of each component (note that in writing Eq. (28) we assume that each component is Gaussian). In these

formulas we have used a “hat” symbol to denote that the W_c and $a_{\ell m}^c$ are those of the specific realization we observe, following [130].

We will assume isotropic white noise in each channel, *i.e.*

$$\langle n_{\ell m}^i (n_{\ell' m'}^j)^* \rangle = w_{(i)}^{-1} \delta^{ij} \delta_{\ell\ell'} \delta_{mm'} . \quad (29)$$

Assuming statistical isotropy, the signal covariance matrix will be block diagonal in harmonic space: therefore the expression for the log-likelihood $L \equiv -2 \log \mathcal{L}$ becomes

$$L = \sum_{\ell} (2\ell + 1) \left\{ \text{Tr} \left[\frac{\sum_{m=-\ell}^{\ell} \Delta_{\ell m}^i (\Delta_{\ell m}^j)^*}{W_c^i C_{\ell}^{cc'} W_{c'}^j + N_{\ell}^{ij}} \right] + \log \det \left[W_c^i C_{\ell}^{cc'} W_{c'}^j + N_{\ell}^{ij} \right] \right\} . \quad (30)$$

In this equation we denote by Tr the trace over the frequency channels, and all terms with i, j indices are understood as matrices. Besides we have defined the noise bias as

$$N_{\ell}^{ij} \equiv N_{\ell}^{(i)} \delta^{ij} = w_{(i)}^{-1} e^{\sigma_{(i)}^2 \ell(\ell+1)} \delta^{ij} , \quad (31)$$

for a gaussian beam of beam-size variance $\sigma_{(i)}$. Eq. (30) is the expression of the CMB likelihood, once we are given a map $\Delta_{\ell m}^i$. In our forecasts, however, we do not construct explicitly a map, but we use the estimator that would be made from such a map, *i.e.*

$$\hat{D}_{\ell}^{ij} = \sum_{m=-\ell}^{\ell} \Delta_{\ell m}^i (\Delta_{\ell m}^j)^* \equiv \hat{W}_c^i \hat{C}_{\ell}^{cc'} \hat{W}_{c'}^j + N_{\ell}^{ij} , \quad (32)$$

where the hats denote the fact that the cosmological parameters are fixed to their “true” values. Therefore our expression for L becomes

$$L = \sum_{\ell} (2\ell + 1) \left\{ \text{Tr} \left[\frac{\hat{W}_c^i \hat{C}_{\ell}^{cc'} \hat{W}_{c'}^j + N_{\ell}^{ij}}{W_c^i C_{\ell}^{cc'} W_{c'}^j + N_{\ell}^{ij}} \right] + \log \det \left[W_c^i C_{\ell}^{cc'} W_{c'}^j + N_{\ell}^{ij} \right] \right\} . \quad (33)$$

Given fiducial cosmological parameters (which we assume are the ones describing the true universe) and the beam and noise specifications of the experiment (that are given in Tab. II for a CORe-like experiment), one can construct the likelihood for CMB anisotropies, and then use it in a Monte Carlo Markov Chain exploration of parameter space.

Eq. (33) simplifies a little if we can consider the case of only one component (the CMB) and forget about foregrounds: however, one has still to take into account both auto- and cross-channel power spectra. For N_c channels with the same noise level, considering both auto and cross power spectra is equivalent to have one frequency channel with an effective noise power spectrum lower by

a factor N_c . One can generalize these considerations to the case of channels with different noise levels. The optimal channel combination results in having an effective noise bias N_{ℓ} given by [131–133]

$$N_{\ell} = \left(\sum_i \frac{1}{N_{\ell}^{(i)}} \right)^{-1} = \left(\sum_i w_{(i)} e^{-\sigma_{(i)}^2 \ell(\ell+1)} \right)^{-1} . \quad (34)$$

In reality the presence of foregrounds limits our ability of extracting the CMB signal from the data, and a full likelihood analysis should take them into account. Fortunately, each component scales differently in frequency (*i.e.*, every foreground has a different shape W_c): therefore it is possible to separate them using maps at different frequencies [134, 135]. This foreground subtraction will be the source of additional noise, depending on the level of foreground removal, which will contribute to the noise bias N_{ℓ} (we refer to [133] for a more detailed analysis). In our forecasts we consider the case where this additional noise is much smaller than the instrumental noise of Eq. (31), so that Eq. (34) is recovered.

Therefore, normalizing the likelihood such that $L = 0$ at the fiducial values of the cosmological parameters, we have that (for BB spectra only)

$$L = \sum_{\ell} (2\ell + 1) \left[-1 + \frac{\hat{C}_{\ell}^{\text{tens}} + \hat{C}_{\ell}^{\text{lens}} + N_{\ell}}{C_{\ell}^{\text{tens}} + C_{\ell}^{\text{lens}} + N_{\ell}} + \log \left(\frac{C_{\ell}^{\text{tens}} + C_{\ell}^{\text{lens}} + N_{\ell}}{\hat{C}_{\ell}^{\text{tens}} + \hat{C}_{\ell}^{\text{lens}} + N_{\ell}} \right) \right] , \quad (35)$$

where the “tens” superscript labels the BB spectrum from primordial tensor modes, and the “lens” superscript labels B -modes due to gravitational lensing. As explained in Sec. III C, delensing will be implemented by rescaling C_{ℓ}^{lens} and $\hat{C}_{\ell}^{\text{lens}}$ as

$$C_{\ell}^{\text{lens}} \rightarrow 0.1 \times C_{\ell}^{\text{lens}} , \quad (36a)$$

$$\hat{C}_{\ell}^{\text{lens}} \rightarrow 0.1 \times \hat{C}_{\ell}^{\text{lens}} . \quad (36b)$$

We will use the likelihood of Eq. (35) for the MCMC exploration of parameter space, with one additional caveat: in the case of a non full-sky experiment (where only part of the sky is observed or can be used for cosmology) not all modes are available for the analysis, and Eq. (33) does not hold. One can capture this effect by introducing the f_{sky} parameter, which reduces the available modes by

$$\sum_{\ell} (2\ell + 1) \rightarrow \sum_{\ell} (2\ell + 1) \times f_{\text{sky}} . \quad (37)$$

We follow this approach in our forecast method (with $f_{\text{sky}} = 0.8$ for the CORe satellite), and we refer the reader to [136] for better approximations.

C. Inflationary models and blue n_t

In this appendix we briefly review two models that can produce blue gravity waves, while keeping the scalar sector in accord with observational constraints.

In the model of [119], the inflaton ϕ is an axion, and the breaking of its shift symmetry $\phi \rightarrow \phi + c$ allows for a coupling with a gauge field A_μ (more precisely with its field strength $F_{\mu\nu}$) given by

$$\mathcal{L} \supset -\frac{\alpha}{4f} \phi F_{\mu\nu} \tilde{F}^{\mu\nu}, \quad (38)$$

where the dual $\tilde{F}_{\mu\nu}$ is $\epsilon_{\mu\nu\rho\sigma} F^{\rho\sigma}$ and f is the axion decay constant. The parameter controlling the strength of gauge field production is

$$\xi \equiv \frac{\alpha \langle \dot{\phi} \rangle}{2fH}, \quad (39)$$

and one can show that the leading contribution to the A_μ occupation numbers goes like $e^{2\pi\xi}/\sqrt{\xi}$. The produced gauge fields will act as a source for tensor modes, and the resulting tensor power spectrum (for the left and right polarizations L and R) will be [137–139]

$$P_t^{L,R}(k) = \frac{H^2}{\pi^2 M_{\text{P}}^2} \left(\frac{k}{k_*} \right)^{n_t} \times \left(1 + 2 \frac{H^2}{M_{\text{P}}^2} f^{L,R}(\xi) e^{4\pi\xi} \right), \quad (40)$$

where the function f_L (f_R) will be of order $4 \times 10^{-7}/\xi^6$

($9 \times 10^{-10}/\xi^6$) at large ξ [139, 140]. We see from Eq. (40) that, in the limit of $\dot{\xi} = 0$, the additional contribution to the tensor power will not give a tilt different from the usual single-field slow-roll result: its only effect will be to enhance the value of r [119]. However ξ is increasing during inflation, and one can show that, in the limit where $\delta_\xi \equiv \dot{\xi}/H\xi$ (the fractional variation per Hubble time of ξ) is small, the tensor tilt will receive a correction $\approx (4\pi\xi - 6)\delta_\xi$ (see also [120]). Therefore, for modestly large values of ξ , there is room to have $0 \lesssim n_t \lesssim \mathcal{O}(1)$.

The model described in [122], instead, considers a coupling of the inflaton to the square of the Weyl tensor, *i.e.*

$$\mathcal{L} \supset f(\phi) \frac{W^2}{M^2}, \quad (41)$$

on top of the slow-roll action. Working out the action for tensor perturbations shows that they have a non-trivial speed of sound c_t . While c_t does not deviate too much from unity, [122] shows that it can still have a sizable time dependence. The fractional change per Hubble time of the tensor speed of sound will give then a contribution to the tensor tilt n_t , proportional to $\sqrt{\epsilon_H}$: therefore the consistency relation of Eq. (24) will not hold in this model. The sign and magnitude of the proportionality factor are determined by the derivative of the function f and from the ratio H^2/M^2 : with suitable choices for the scale of variation of f and for the scale M , the overall contribution can lead to blue tilt.

-
- [1] P. de Bernardis *et al.* [Boomerang Collaboration], *Nature* **404**, 955 (2000).
 - [2] D. J. Eisenstein *et al.* [SDSS Collaboration], *Astrophys. J.* **633**, 560 (2005).
 - [3] G. Hinshaw *et al.* [WMAP Collaboration], *Astrophys. J. Suppl.* **208**, 19 (2013).
 - [4] R. Adam *et al.* [Planck Collaboration], arXiv:1502.01582 [astro-ph.CO].
 - [5] A. H. Guth, *Phys. Rev. D* **23**, 347 (1981).
 - [6] A. D. Linde, *Phys. Lett. B* **108**, 389 (1982).
 - [7] A. Albrecht and P. J. Steinhardt, *Phys. Rev. Lett.* **48**, 1220 (1982).
 - [8] D. Baumann, arXiv:0907.5424 [hep-th].
 - [9] M. Kamionkowski and E. D. Kovetz, arXiv:1510.06042 [astro-ph.CO].
 - [10] N. Aghanim *et al.* [Planck Collaboration], [arXiv:1507.02704 [astro-ph.CO]].
 - [11] P. A. R. Ade *et al.* [BICEP2 and Planck Collaborations], *Phys. Rev. Lett.* **114**, no. 10, 101301 (2015).
 - [12] K. Array *et al.* [BICEP2 s Collaboration], arXiv:1510.09217 [astro-ph.CO].
 - [13] P. A. R. Ade *et al.* [Planck Collaboration], arXiv:1502.02114 [astro-ph.CO].
 - [14] B. Allen, In *Les Houches 1995, Relativistic gravitation and gravitational radiation* 373-417.
 - [15] M. Maggiore, *Phys. Rept.* **331**, 283 (2000).
 - [16] C. Cutler and K. S. Thorne, gr-qc/0204090.
 - [17] C. J. Moore, R. H. Cole and C. P. L. Berry, *Class. Quant. Grav.* **32** (2015) 1, 015014 doi:10.1088/0264-9381/32/1/015014
 - [18] B. P. Abbott *et al.* [LIGO Scientific Collaboration], *Rept. Prog. Phys.* **72**, 076901 (2009).
 - [19] J. Abadie *et al.* [LIGO Collaboration], *Nature Phys.* **7**, 962 (2011).
 - [20] F. Acernese *et al.* [VIRGO Collaboration], *Class. Quant. Grav.* **22**, S869 (2005).
 - [21] F. Acernese *et al.* [VIRGO Collaboration], *Class. Quant. Grav.* **32**, no. 2, 024001 (2015).
 - [22] P. Amaro-Seoane *et al.*, *GW Notes* **6**, 4 (2013).
 - [23] P. Amaro-Seoane *et al.*, *Class. Quant. Grav.* **29**, 124016 (2012).
 - [24] S. Kawamura *et al.*, *Class. Quant. Grav.* **23**, S125 (2006).
 - [25] S. Kawamura *et al.*, *Class. Quant. Grav.* **28**, 094011 (2011).
 - [26] J. Crowder and N. J. Cornish, *Phys. Rev. D* **72**, 083005 (2005).
 - [27] R. D. Ferdman *et al.*, *Class. Quant. Grav.* **27**, 084014

- (2010).
- [28] D. J. Fixsen, E. S. Cheng, J. M. Gales, J. C. Mather, R. A. Shafer and E. L. Wright, *Astrophys. J.* **473**, 576 (1996).
- [29] A. Ota, T. Takahashi, H. Tashiro and M. Yamaguchi, *JCAP* **1410**, no. 10, 029 (2014).
- [30] J. Chluba, L. Dai, D. Grin, M. Amin and M. Kamionkowski, *Mon. Not. Roy. Astron. Soc.* **446**, 2871 (2015).
- [31] W. Hu and J. Silk, *Phys. Rev. D* **48**, 485 (1993).
- [32] J. Chluba, R. Khatri and R. A. Sunyaev, *Mon. Not. Roy. Astron. Soc.* **425**, 1129 (2012).
- [33] E. Pajer and M. Zaldarriaga, *JCAP* **1302**, 036 (2013).
- [34] W. Hu, D. Scott and J. Silk, *Astrophys. J.* **430**, L5 (1994).
- [35] J. Chluba, A. L. Erickcek and I. Ben-Dayan, *Astrophys. J.* **758**, 76 (2012).
- [36] G. Mangano, G. Miele, S. Pastor and M. Peloso, *Phys. Lett. B* **534**, 8 (2002).
- [37] G. Mangano, G. Miele, S. Pastor, T. Pinto, O. Pisanti and P. D. Serpico, *Nucl. Phys. B* **729**, 221 (2005).
- [38] R. Bowen, S. H. Hansen, A. Melchiorri, J. Silk and R. Trotta, *Mon. Not. Roy. Astron. Soc.* **334**, 760 (2002).
- [39] Z. Hou, R. Keisler, L. Knox, M. Millea and C. Reichardt, *Phys. Rev. D* **87**, 083008 (2013).
- [40] Y. I. Izotov, T. X. Thuan and N. G. Guseva, *Mon. Not. Roy. Astron. Soc.* **445**, no. 1, 778 (2014).
- [41] A. Mucciarelli, L. Lovisi, B. Lanzoni, and F. R. Ferraro, *Astrophys. J.* **786**, no. 1, 14 (2014).
- [42] R. Cooke, M. Pettini, R. A. Jorgenson, M. T. Murphy and C. C. Steidel, *Astrophys. J.* **781** (2014) 1, 31.
- [43] R. H. Cyburt, B. D. Fields and K. A. Olive, *Astropart. Phys.* **17**, 87 (2002).
- [44] K. Ichikawa, T. Sekiguchi and T. Takahashi, *Phys. Rev. D* **78**, 043509 (2008).
- [45] T. Damour and A. Vilenkin, *Phys. Rev. Lett.* **85**, 3761 (2000).
- [46] S. Olmez, V. Mandic and X. Siemens, *Phys. Rev. D* **81**, 104028 (2010).
- [47] C. Ungarelli, P. Corasaniti, R. A. Mercer and A. Vecchio, *Class. Quant. Grav.* **22**, S955 (2005).
- [48] T. L. Smith, H. V. Peiris and A. Cooray, *Phys. Rev. D* **73**, 123503 (2006).
- [49] S. Chongchitnan and G. Efstathiou, *Phys. Rev. D* **73**, 083511 (2006).
- [50] T. L. Smith, E. Pierpaoli and M. Kamionkowski, *Phys. Rev. Lett.* **97**, 021301 (2006).
- [51] L. A. Boyle and A. Buonanno, *Phys. Rev. D* **78**, 043531 (2008).
- [52] A. Stewart and R. Brandenberger, *JCAP* **0808**, 012 (2008).
- [53] R. Camerini, R. Durrer, A. Melchiorri, A. Riotto, R. Durrer, A. Melchiorri and A. Riotto, *Phys. Rev. D* **77** (2008) 101301 [arXiv:0802.1442 [astro-ph]].
- [54] I. Sendra and T. L. Smith, *Phys. Rev. D* **85**, 123002 (2012).
- [55] E. Di Valentino, A. Melchiorri and L. Pagano, *Int. J. Mod. Phys. D* **20** (2011) 1183.
- [56] M. Gerbino, A. Marchini, L. Pagano, L. Salvati, E. Di Valentino and A. Melchiorri, *Phys. Rev. D* **90**, no. 4, 047301 (2014).
- [57] S. Henrot-Versille *et al.*, *Class. Quant. Grav.* **32**, no. 4, 045003 (2015).
- [58] P. D. Meerburg, R. Hložek, B. Hadzhiyska and J. Meyers, *Phys. Rev. D* **91**, no. 10, 103505 (2015).
- [59] Q. G. Huang and S. Wang, *JCAP* **1506**, no. 06, 021 (2015).
- [60] T. Nakama and T. Suyama, *Phys. Rev. D* **92**, no. 12, 121304 (2015).
- [61] L. Pagano, L. Salvati and A. Melchiorri, arXiv:1508.02393 [astro-ph.CO].
- [62] Q. G. Huang, S. Wang and W. Zhao, *JCAP* **1510**, no. 10, 035 (2015).
- [63] A. Kogut *et al.*, *JCAP* **1107**, 025 (2011).
- [64] T. Matsumura *et al.*, *Journal of Low Temperature Physics* September 2014, Volume 176, Issue 5-6, pp 733-740.
- [65] F. R. Bouchet *et al.* [CORe Collaboration], arXiv:1102.2181 [astro-ph.CO].
- [66] J. Aasi *et al.* [LIGO Scientific Collaboration], *Class. Quant. Grav.* **32**, 074001 (2015).
- [67] E. Calabrese *et al.*, *JCAP* **1408** (2014) 010.
- [68] M. D. Niemack *et al.*, *Proc. SPIE Int. Soc. Opt. Eng.* **7741**, 77411S (2010).
- [69] Besides, if tensor modes are actually detected, the bounds that one will obtain on the tensor tilt will be prior-independent: see Sec. IV for a discussion.
- [70] J. Errard, S. M. Feeney, H. V. Peiris and A. H. Jaffe, arXiv:1509.06770 [astro-ph.CO].
- [71] J. E. Lidsey, A. R. Liddle, E. W. Kolb, E. J. Copeland, T. Barreiro and M. Abney, *Rev. Mod. Phys.* **69**, 373 (1997).
- [72] L. A. Boyle and P. J. Steinhardt, *Phys. Rev. D* **77**, 063504 (2008).
- [73] Y. Watanabe and E. Komatsu, *Phys. Rev. D* **73**, 123515 (2006).
- [74] J. R. Pritchard and M. Kamionkowski, *Annals Phys.* **318**, 2 (2005).
- [75] This condition is necessary for ρ_{GW} to redshift as radiation (*i.e.* as a^{-4}), which in turn has been used in deriving Eqs. (10) and (11).
- [76] T. L. Smith, “The gravity of the situation,”
- [77] D. Jeong, J. Pradler, J. Chluba and M. Kamionkowski, *Phys. Rev. Lett.* **113**, 061301 (2014).
- [78] J. Chluba and R. A. Sunyaev, *Mon. Not. Roy. Astron. Soc.* **419**, 1294 (2012).
- [79] S. Weinberg, *Astrophys. J.* **168**, 175 (1971).
- [80] N. Kaiser, *Mon. Not. Roy. Astron. Soc.* **202**, 1169 (1983).
- [81] W. Hu and M. J. White, *Phys. Rev. D* **56**, 596 (1997).
- [82] This approximation works well in the tight-coupling regime which, again, is a valid hypothesis at the redshifts when μ -distortions are generated.
- [83] S. Weinberg, *Phys. Rev. D* **69**, 023503 (2004).
- [84] R. Khatri, R. A. Sunyaev and J. Chluba, *Astron. Astrophys.* **540**, A124 (2012).
- [85] When one is dealing with small perturbations of the Planck spectrum, linear theory can be used: in the linear limit, then, it is possible to show that for large enough frequencies (*i.e.* away from the Rayleigh-Jeans tail) a small μ -distortion with negative sign is a good approximation.
- [86] S. Detweiler, *Astrophys. J.* **234**, 1100 (1979).
- [87] M. Pitkin, S. Reid, S. Rowan and J. Hough, *Living Rev. Rel.* **14**, 5 (2011).
- [88] R. X. Adhikari, *Rev. Mod. Phys.* **86**, 121 (2014).
- [89] A. Lewis and S. Bridle, *Phys. Rev. D* **66**, 103511 (2002).
- [90] A. Lewis, *Phys. Rev. D* **87**, no. 10, 103529 (2013).

- [91] M. Kawasaki, K. Kohri and N. Sugiyama, Phys. Rev. Lett. **82**, 4168 (1999).
- [92] M. Kawasaki, K. Kohri and N. Sugiyama, Phys. Rev. D **62**, 023506 (2000).
- [93] P. F. de Salas, M. Lattanzi, G. Mangano, G. Miele, S. Pastor and O. Pisanti, arXiv:1511.00672 [astro-ph.CO].
- [94] P. A. R. Ade *et al.* [Planck Collaboration], arXiv:1502.01589 [astro-ph.CO].
- [95] F. Beutler *et al.*, Mon. Not. Roy. Astron. Soc. **416**, 3017 (2011).
- [96] A. J. Ross, L. Samushia, C. Howlett, W. J. Percival, A. Burden and M. Manera, Mon. Not. Roy. Astron. Soc. **449**, no. 1, 835 (2015).
- [97] L. Anderson *et al.* [BOSS Collaboration], Mon. Not. Roy. Astron. Soc. **441**, no. 1, 24 (2014).
- [98] L. Salvati, L. Pagano, R. Consiglio and A. Melchiorri, arXiv:1507.07243 [astro-ph.CO].
- [99] J. Aasi *et al.* [LIGO Scientific and VIRGO Collaborations], Phys. Rev. Lett. **113**, no. 23, 231101 (2014).
- [100] L. Lentati *et al.*, Mon. Not. Roy. Astron. Soc. **453**, 2576 (2015).
- [101] A. Lewis, Phys. Rev. D **71**, 083008 (2005).
- [102] <http://www.core-mission.org>.
- [103] M. Zaldarriaga and U. Seljak, Phys. Rev. D **58** (1998) 023003.
- [104] K. M. Smith *et al.*, AIP Conf. Proc. **1141** (2009) 121.
- [105] L. Knox and Y. S. Song, Phys. Rev. Lett. **89**, 011303 (2002).
- [106] M. Kesden, A. Cooray and M. Kamionkowski, Phys. Rev. Lett. **89**, 011304 (2002).
- [107] U. Seljak and C. M. Hirata, Phys. Rev. D **69**, 043005 (2004).
- [108] K. M. Smith, D. Hanson, M. LoVerde, C. M. Hirata and O. Zahn, JCAP **1206**, 014 (2012).
- [109] P. Creminelli, D. L. Nacir, M. Simonović, G. Trevisan and M. Zaldarriaga, arXiv:1502.01983 [astro-ph.CO].
- [110] We also see from Fig. 2 that this argument does not hold for a tensor-to-scalar ratio too small, since in that case the primordial B -mode angular spectrum C_ℓ^{tens} is swamped by noise too soon, and the sensitivity to n_t is lost even if we reduce the power of lensing B -modes.
- [111] As shown in [109], while a value of r of order 10^{-3} will not be probed by future ground-based experiments, future satellite missions will be able to detect it with a σ_r/r of order 10^{-1} .
- [112] This mechanism is the same that was proposed in [56] to explain the tension between *Planck* data and the claim from the BICEP2 collaboration of $r \approx 0.2$ at 0.05 Mpc^{-1} .
- [113] Since using the BK14 dataset does not change significantly the best-fit of the combined analysis with LIGO-Virgo, we will not consider the forecast for *Planck* + BK14 + AdvLIGO.
- [114] Which, we note, are obtained with a “just CMB” dataset, *i.e.* by looking only at the effects of primordial tensor modes on CMB temperature and polarization anisotropies.
- [115] T. Kobayashi, M. Yamaguchi and J. Yokoyama, Phys. Rev. Lett. **105**, 231302 (2010).
- [116] P. Creminelli, M. A. Luty, A. Nicolis and L. Senatore, JHEP **0612**, 080 (2006).
- [117] Y. Wang and W. Xue, JCAP **1410**, no. 10, 075 (2014).
- [118] L. Senatore, E. Silverstein and M. Zaldarriaga, JCAP **1408**, 016 (2014).
- [119] N. Barnaby, E. Pajer and M. Peloso, Phys. Rev. D **85**, 023525 (2012).
- [120] S. Mukohyama, R. Namba, M. Peloso and G. Shiu, JCAP **1408**, 036 (2014).
- [121] N. Kaloper, M. Kleban, A. E. Lawrence and S. Shenker, Phys. Rev. D **66**, 123510 (2002).
- [122] D. Baumann, H. Lee and G. L. Pimentel, arXiv:1507.07250 [hep-th].
- [123] B. A. Benson *et al.* [SPT-3G Collaboration], Proc. SPIE Int. Soc. Opt. Eng. **9153**, 91531P (2014).
- [124] On the other hand, we note that any excess in radiation energy density could be due either to primordial gravitational waves or to additional light particles, not predicted by the Standard Model of particle physics.
- [125] In the slow-roll approximation, one can write the fractional change of $\epsilon_H \equiv \epsilon$ per e-fold of inflation as
- $$\epsilon \approx \epsilon_* + \left. \frac{d\epsilon}{dN} \right|_* \Delta N .$$
- Recalling that
- $$-(n_s - 1)|_* = 2\epsilon_* - \left. \frac{1}{\epsilon_*} \frac{d\epsilon}{dN} \right|_* ,$$
- one finds $\Delta\epsilon/\epsilon_* \approx (0.04 + r_*/8) \times \Delta N \approx 0.04 \times \Delta N$. For $\Delta N \approx \log k_{\text{LIGO}}/k_{\text{CMB}} \approx \log 10^{19}$, one has a fractional change in the slow-roll parameter ϵ of order 1.7.
- [126] M. Remazeilles, C. Dickinson, H. K. K. Eriksen and I. K. Wehus, arXiv:1509.04714 [astro-ph.CO].
- [127] P. D. Lasky *et al.*, arXiv:1511.05994 [astro-ph.CO].
- [128] P. Adshead, R. Easther, J. Pritchard and A. Loeb, JCAP **1102**, 021 (2011).
- [129] L. Perotto, J. Lesgourgues, S. Hannestad, H. Tu and Y. Y. Y. Wong, JCAP **0610**, 013 (2006).
- [130] J. R. Bond, A. H. Jaffe and L. E. Knox, Astrophys. J. **533** (2000) 19.
- [131] J. R. Bond, G. Efstathiou and M. Tegmark, Mon. Not. Roy. Astron. Soc. **291**, L33 (1997).
- [132] G. Efstathiou and J. R. Bond, Mon. Not. Roy. Astron. Soc. **304** (1999) 75.
- [133] L. Verde, H. Peiris and R. Jimenez, JCAP **0601**, 019 (2006).
- [134] M. P. Hobson, A. W. Jones, A. N. Lasenby and F. R. Bouchet, Mon. Not. Roy. Astron. Soc. **300** (1998) 1.
- [135] C. Baccigalupi, F. Perrotta, G. De Zotti, G. F. Smoot, C. Burigana, D. Maino, L. Bedini and E. Salerno, Mon. Not. Roy. Astron. Soc. **354** (2004) 55.
- [136] B. D. Wandelt, E. Hivon and K. M. Gorski, Phys. Rev. D **64** (2001) 083003.
- [137] N. Barnaby and M. Peloso, Phys. Rev. Lett. **106**, 181301 (2011).
- [138] L. Sorbo, JCAP **1106**, 003 (2011).
- [139] N. Barnaby, R. Namba and M. Peloso, JCAP **1104**, 009 (2011).
- [140] We note that, since $f^L \neq f^R$, the primordial gravitational waves produced by this mechanism will be parity violating.